JET–P(98)44

F X Söldner et al

Approach to Steady-state High Performance in DD and DT with Optimised Shear on JET

JET–P(98)44

Approach to Steady-state High Performance in DD and DT with Optimised Shear on JET

F X Söldner, Y F Baranov, D V Bartlett, C D Challis, H Chen[1], I Coffey, G A Cottrell, A C Ekedahl[2], C Gormezano, C M Greenfield[3], G T A Huysmans, E A Lazarus[4], X Litaudon[5], T C Luce[3], B W Rice[6], V Parail, F Rochard[5], P Schild, AC C Sips, E J Strait[3], B J D Tubbing, M von Hellermann, M R Wade[4], D J Ward.

JET Joint Undertaking, Abingdon, Oxfordshire, OX14 3EA,
[1]Imperial College, London, UK.
[2]Chalmers University, Gothenburg, Sweden.
[3]General Atomics, San Diego, USA.
[4]Oak Ridge Nat. Lab., USA.
[5]CEA Cadarache, France.
[6]Lawrence Livermore Nat. Lab., USA.

Preprint of a Paper to be submitted for publication in Nuclear Fusion

December 1998

ABSTRACT

Steady-state high performance with improved core confinement and sustainable plasma edge conditions has been approached on JET in a Double Barrier (DB) mode. The DB mode combines an internal transport barrier of the Optimised Shear regime with an edge transport barrier of an ELM´y H-mode regime. Improved confinement with an H-factor $H^{ITER-89} \approx 2$ has been maintained for four energy confinement times. Ion and electron temperature profiles remain peaked in the DB mode, while the density profile is broad and similar in shape to the ELM´y H-mode profile. The energy confinement improves across the whole plasma cross section, and the ion heat conductivity falls to the neo-classical level in the core. Particle transport studies show that impurity accumulation can be avoided in the DB mode. In deuterium-tritium discharges the DB mode has attained a fusion gain of $Q \approx 0.4$, producing 6.8 MW fusion power, compared with $Q \approx 0.2$ in the conventional sawtoothing ELMy H-mode. The ELM´s are more benign, with the amplitude an order of magnitude smaller in the Optimised Shear ELM´y H-mode. The DB mode has a high potential to improve performance in reactor relevant conditions.

1. INTRODUCTION

Fusion performance and energy confinement in tokamak plasma discharges have been improved considerably over recent years in new operation regimes with control of the plasma current profile. Peaked pressure profiles with improved core confinement have been obtained in the PEP regime on JET [1]. Strong improvement in ion energy confinement inside an internal transport barrier has been observed with a hollow current profile resulting in negative central shear on TFTR [2], DIII-D [3] and JT-60U [4]. JET has obtained similar results with low central magnetic shear [5]. Control of the magnetic shear also gave the record machine performance in deuterium discharges in DIII-D [6] and JET [7]. The salient ingredient to these high performance regimes is the formation of an internal transport barrier as it has been found also in the high-$ß_p$ regime on JT-60U [8]. In these cases high performance could be achieved only transiently. Gradual roll-over or disruptive termination have been caused by MHD instabilities arising from the continuing evolution of current and pressure profiles. In this paper first results are presented on high performance DD and DT discharges in JET approaching steady-state conditions with control of the shear. The modes of operation with optimisation of the magnetic shear are described in Section 2. Extended performance with internal transport barriers in L-mode is presented in Section 3. Sustained high performance and the approach to steady-state conditions with a Double Barrier (DB) mode, combining internal and external transport barriers in ELMy H-mode, is discussed in detail in Section 4. Profile evolution, energy and particle transport and MHD stability in the DB mode operation regime are analysed in this Section. The DB mode is finally compared with the conventional ELMy H-mode presently considered for the nominal ignition scenario on ITER. The results are summarised in Section 5.

2. OPERATION REGIME OF OPTIMISED SHEAR DISCHARGES

High performance in the Optimised Shear regime on JET has been achieved with a tight control of current and pressure profiles [9]. Lower Hybrid Current Drive (LHCD) with low power of ~ 1 MW coupled is applied in the initial phase of plasma formation for 0.8 - 1.5 s to slow down current penetration and provide a broad target current profile. Subsequent Ion Cyclotron Resonance Heating (ICRH) with 1-2 MW maintains high electron temperatures without further changing strongly the current distribution. High power heating with central deposition from Neutral Beam Injection (NBI) and ICRH is then applied at the end of the plasma current ramp at low target density. With a total heating power in excess of ~15 MW an internal transport barrier can be formed in these conditions. Ion and electron temperatures, the density and the toroidal rotation profiles are peaking in the central plasma region. The steep gradient zone subsequently expands slowly outwards.

2.1 Performance Evolution

After formation of an internal transport barrier (ITB) the Optimised Shear discharges can evolve along four different routes as displayed in Fig. 1.

High performance has been achieved by preserving an L-mode edge, preventing an H-mode transition by a continuing current ramp, strong pumping of the scrape-off layer and increasing triangularity. In this case the temperature and density profiles are continuously peaking in the core and the fusion rate is continuously rising as shown in Fig. 1a. Very high central ion temperatures up to 40 keV and strong ITBs could be achieved in this regime in deuterium-tritium (DT) plasmas [10]. But the strong rise of the pressure gradient finally destabilises a rapidly growing pressure driven global kink mode which leads to a disruption [11]. Control of the pressure profile by real time control of central power deposition from ICRH on the fusion rate avoids a disruption as shown with the discharge in Fig. 1b. After an extended L-mode phase with an ITB present, the plasma edge transits into an ELM-free H-mode as seen from the sudden drop in the D_α emission. In the ELM-free H-mode, however, neutron rate and central ion temperature saturate and roll over before a giant ELM finally terminates the high performance phase. Both, edge pressure pedestal and internal transport barrier are destroyed by this large ELM. A phase with violent ELMs follows and discharges passing along this route never recover to the preceding good confinement conditions due to impurity influx and current and pressure profile re-distribution.

Internal transport barriers can be maintained into quasi steady-state conditions in two possible ways, either with an L-mode edge or with an ELMy H-mode edge as shown in Fig.'s 1c, d. In pulse No. 40406 (Fig. 1c) an ITB forms just at the time of reduction of the ICRH power. With reduced central power deposition the core pressure gradient rises more slowly. It comes to a halt at 7.4 s. Central ion temperature and fusion rate saturate at this time. They change then only slightly during the following ~ 0.9 s until the end of high power heating. This flat-top

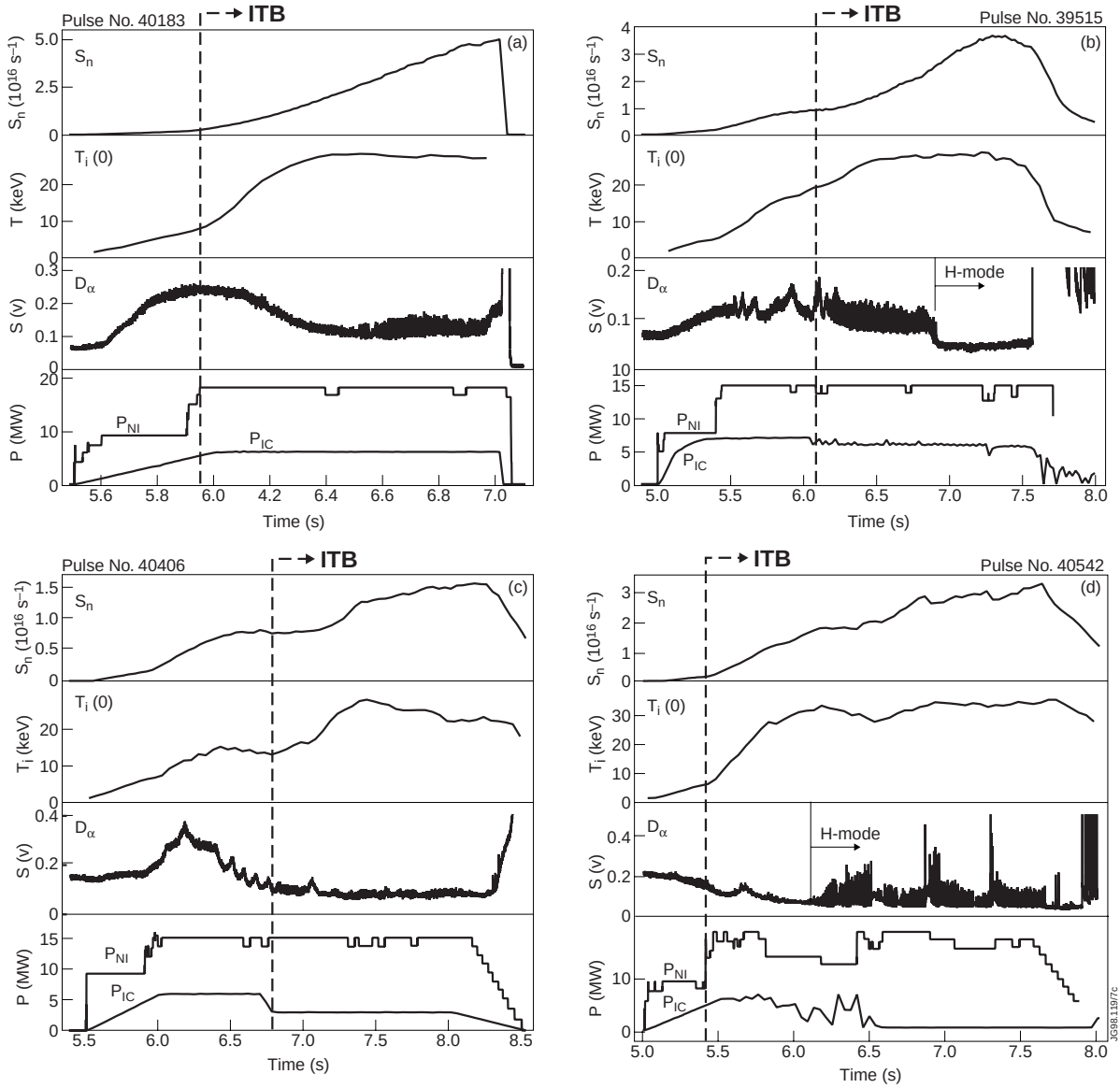

Fig.1: Overview of fusion rate, central ion temperature, D_α emission and heating powers in four types of discharges with ITBs in L-mode (a,c) and H-mode (b,d). I_p = 3.25 MA, B_t = 3.45 T.

period corresponds to about two energy confinement times. The ITB is stabilised in this discharge by MHD activity in the gradient zone. This imposes, however, limitations on the performance, and the discharge remains clamped at about one third of the fusion rate attained at the end of the continuous rise in pulse No. 40183 (Fig. 1a). The other alternative route is a transition of the plasma edge to ELMy H-mode as shown in Fig. 1d. In this case excessive pressure peaking could be avoided. High central ion temperature and fusion rate, still slowly growing due to continuing fuelling from NBI, could then be maintained until the end of the high power heating phase, for about four energy confinement times.

The radial extent of the improved core confinement region and the respective ITB quality for the four types of discharge scenarios are seen from the ion temperature profiles in Fig. 2. The narrowest zone with high ion temperatures is found in the quasi steady-state L-mode with ITB (pulse No. 40406 of Fig. 1c). A moderate gradient inside one third of the plasma radius is

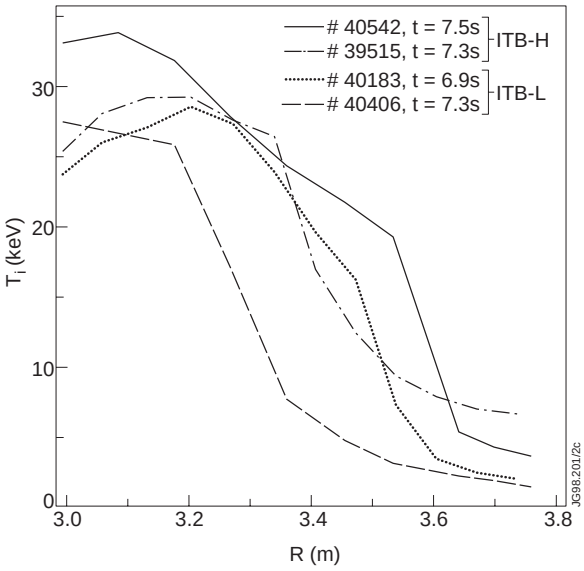

Fig.2: Ion temperature profiles for the four types of discharges with ITBs in Fig. 1 at the times of maximum central values.

restrained in growth by persisting MHD activity outside this region. Wider zones of high ion temperature inside a steep gradient at about half plasma radius are obtained with the long quiet L-mode phase in pulse No. 40183 (Fig. 1a) and the sequence of L-and ELM-free H-mode phases in pulse No. 39515 (Fig. 1b). But the steep gradient in the foot of the ITB in pulse No. 40183 finally causes the disruptive growth of the pressure driven kink mode. The highest central values and the largest expansion of the ITB are achieved in the ELMy H-mode discharge No. 40542 (Fig. 1d). In the ITB/ELMy H-mode the edge pedestal in the ion temperature profile is about a factor 2 higher than the edge temperatures in the ITB/L-mode cases but only half the value of the ITB/ELM-free H-mode. This provides also the perspective for better MHD stability of the ITB/ELMy H-mode due to a lower edge pressure gradient.

The development of the ITB in the four types of discharges is documented in Fig. 3. The outer edge of the ITB is characterised by the maximum change in the gradient of the temperature profile. As the ITB formation is most obvious in the ion temperature profile, the outer footpoint of the ITB is defined here by the maximum of the second radial derivative of the ion temperature. The time evolution of this outer footpoint shows a radial expansion of the ITB in all cases. The ITB moves outward, however, only during the L-mode phase. After the transition to the H-mode the expansion is stopped, both in ELM-free (pulse No. 39515) and ELMy phases (pulse No. 40542). With the long ELMy H-mode, however, a very wide improved core with the ITB at two thirds of the plasma radius can be stabilised.

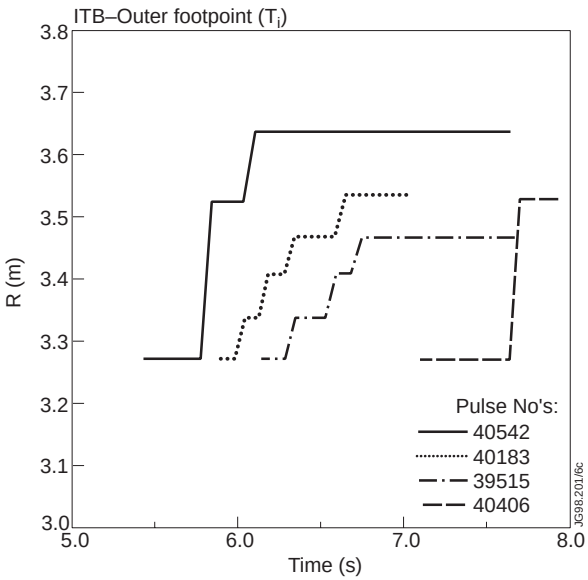

Fig.3: Temporal evolution of the outer footpoint of the ITB in the four types of discharges with ITBs in Fig. 1.

2.2 MHD Activity

The performance in the Optimised Shear regime is strongly influenced by the MHD activity. Three types of modes are characteristic for discharges with ITBs [12]. The most dangerous is a global n=1 kink mode driven by the strong pressure profile peaking. It grows rapidly, locks and

leads to a disruptive termination of most high performance discharges with an ITB and an L-mode edge. A mode with a similar pattern, located in the steep pressure gradient region, usually correlates with the transition from L to ELM-free H-mode in presence of an ITB. The frequency starts in the range 10-25 kHz and may increase up to about 100 kHz during the ELM-free H-mode. The amplitude is slowly growing while at the same time the ITB quality is gradually degrading as seen from a broadening of the gradient region, a shrinking of the ITB radius and a drop of the ion temperature inside the ITB. Finally, a peculiar low frequency (0.2-0.7 kHz) mode located near the separatrix appears in the L-mode phases of Optimised Shear discharges [13]. The amplitude saturates and no deleterious impact on confinement is seen from this mode.

The characteristic MHD behaviour in the four Optimised Shear operation regimes is summarised in an overview of magnetic pick-up signals in Fig. 4 for the discharges of Fig. 1.

The high performance ITB/L-mode with disruptive termination (Fig. 4a) contains a continuous low frequency mode also seen from the spread in the D_α emission resembling the ELM signature (Fig. 1a). A rapidly growing high frequency mode leads to the final disruption. The frequency integrated oscillation amplitude dB_Θ/dt is increasing throughout the whole ITB phase indicating the transient nature of this regime.

The ITB discharge with staggered L and ELM-free H-mode phases in Fig. 4b contains again the low frequency mode during the L-mode phase. With the transition to the ELM-free H-mode this mode disappears and the high frequency mode starts growing. The continuous growth of the frequency integrated signal shows that an increasing MHD activity with a resulting degradation in core confinement accompanies the ELM-free H-mode phase which is finally terminated by a giant ELM.

In the quasi steady-state ITB/L-mode of Fig. 4c both, low and high frequency modes grow and decrease occasionally in amplitude. The sudden appearance of the high frequency mode (25 kHz) around 8 s resembles disruptive terminations in other ITB/L-mode discharges. This indicates the marginal balance between ITB sustainment and MHD mode destabilisation in this mode of operation.

The ITB/ELMy H-mode in Fig. 4d shows only short bursts of the low frequency mode. The high frequency mode (60 kHz) grows after the reduction in ELM amplitude at 6.5 s but saturates then for the whole duration of high power heating until 7.5 s. With the right ELM frequency and amplitude the ITB can therefore be stabilised at high performance.

Internal transport barriers have been maintained into steady-state conditions for several energy confinement times with two scenarios. In discharges with an L-mode edge disruptive terminations could be avoided when localised MHD activity in the foot of the ITB prevented excessive pressure peaking. The other route combines an ITB with an ELMy H-mode edge which constrains core pressure peaking and also improves confinement in peripheral plasma regions. This mode therefore provides simultaneously improved stability and confinement.

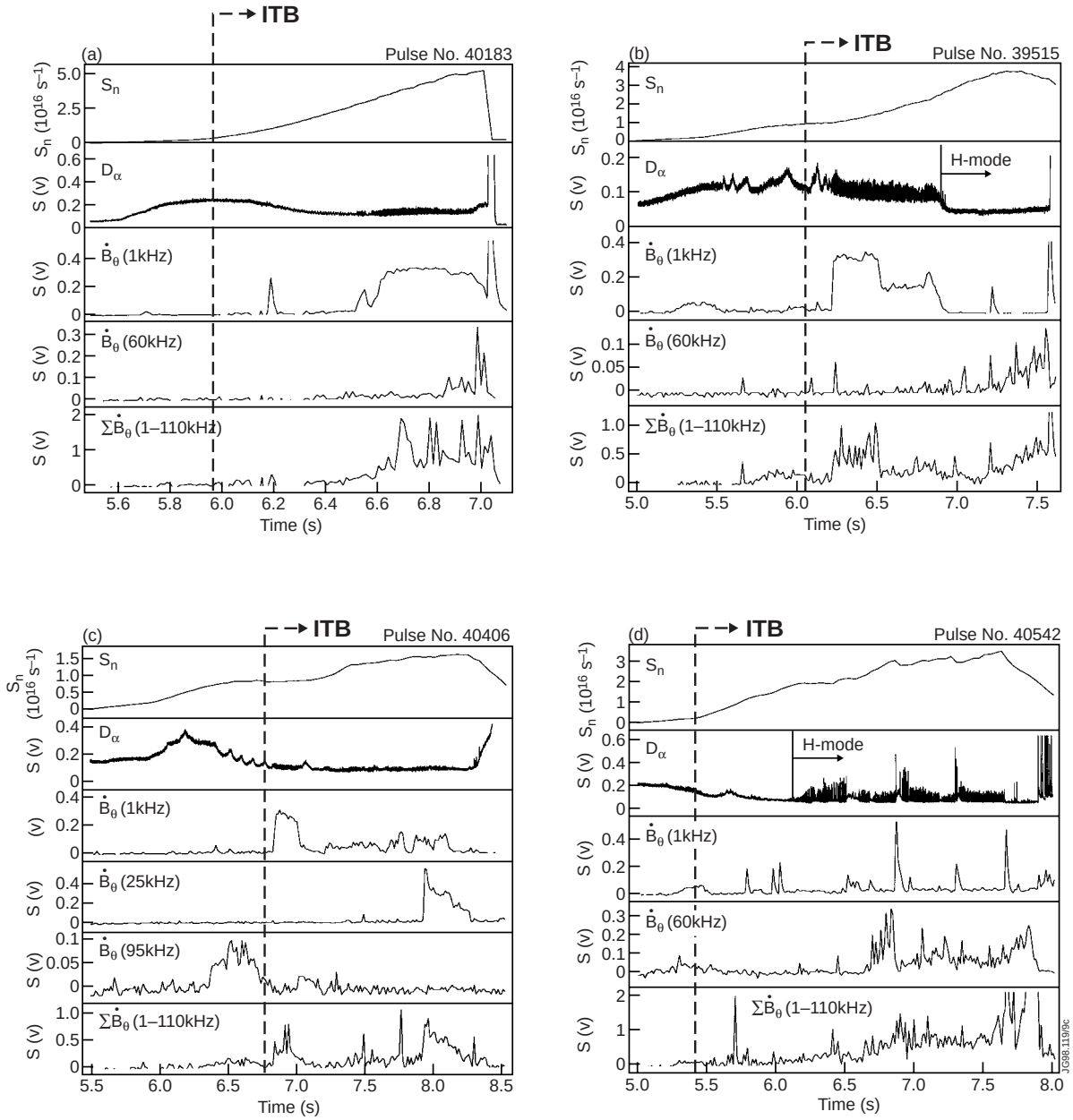

Fig.4: Overview of the MHD activity in the four types of discharges with ITBs as of Fig.1. Fusion neutron rate S_n, D_α emission and frequency filtered magnetic pick-up signals.

3. SUSTAINED PERFORMANCE IN INTERNAL TRANSPORT BARRIER L-MODE

Extended L-mode phases with strong density peaking after the formation of an ITB have allowed to achieve the highest fusion rate in the Optimised Shear regime on JET [7]. The operation in L-mode has also the attraction of stable edge conditions and avoids peak transient power loads onto the divertor plates. An effort has been made therefore to stabilise ITB/L-mode discharges at high performance level.

The experiments on JET aimed mainly at controlling the pressure profile by feedback control of the power deposition profile, varying the composition from NBI and ICRH [9]. Reduction of the central power deposition from ICRH was instrumental to enter a long sustained

L-mode phase with ITB in the discharge discussed above with Fig. 1c. Ion and electron temperature there are rising after the reduction of total power input at 6.8 s first in the plasma centre. The zone of improved confinement expands then. The expansion slows down and the profiles approach steady-state conditions towards the end of the high power heating phase. The D_α emission remains at low amplitude during the whole ITB/L-mode phase. This indicates a low level of recycling in the main chamber due to reduced particle losses from the plasma. D_α emission and the underlying recycling rate are comparable with the conditions in ELM-free H-mode. Here this is attained with the combination of an L-mode edge with the internal transport barrier, reducing strongly the radial outflow of particles from the core.

Enhanced performance in L-mode has been extended over two energy confinement times after the ITB formation by changing the composition of the heating power in the discharge shown in Fig. 5. The NBI power has been stepped down in this case in order to allow to maintain a higher central power deposition from ICRH. The resulting peaking in the input power deposition profile simulates conditions in the initial phase of growing fusion power production. Core heating from α-particles will take over in this phase from the external power input. Steep pressure gradients could be maintained stable in this case. But the ITB starts shrinking without obvious signs of MHD activity from 6.5 s while the core temperatures are still slightly rising. A transition to ELM-free H-mode at 7 s is possibly triggered by a short transient reduction in the ICRH power. The central ion temperature begins falling immediately after the H-mode transition and the ITB gradually decays until large ELMs finally destroy it completely. The H-mode appears to be the result of a core confinement degradation and the resulting enhanced radial outflow of energy to the plasma periphery. The total power input in the ITB/L-mode phase obviously has been marginal in this discharge and already a slight reduction can lead to an erosion of the ITB and the improved core confinement region.

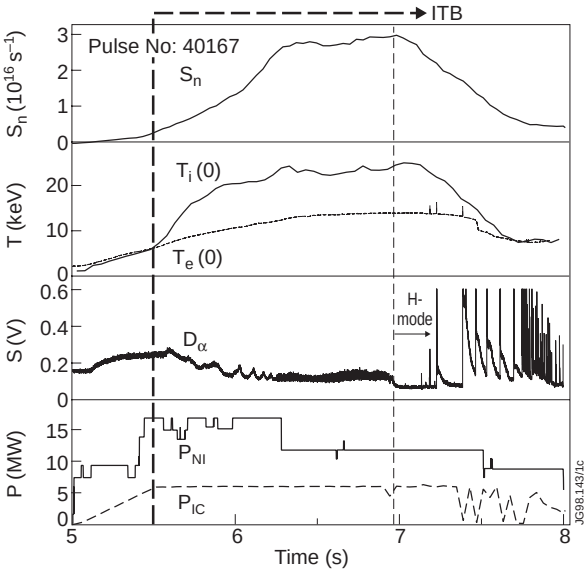

Fig.5: Optimised Shear discharge with an extended L-mode phase after the formation of an ITB.

The path between excessive pressure peaking with too high central heating power and irrecoverable loss of the ITB after a reduction of power input is very narrow in ITB/L-mode discharges. Very fine control of the power deposition profile and the total power input are required to extend the high performance phase. The attraction of combining the high confinement core inside an ITB with a low pressure L-mode edge, however, calls for a continuing development of this operation mode using profile control.

4. SUSTAINED PERFORMANCE IN DOUBLE BARRIER H-MODE

4.1 Limitations by L-mode Back-transitions

ITBs could be combined with ELMy H-modes either with an H-mode transition after the ITB formation or in reverse order with the build-up of an ITB in a fully developed H-mode. Examples for both sequences are shown in Fig. 6. Pulse No. 40206 (Fig. 6a) has an H-mode transition

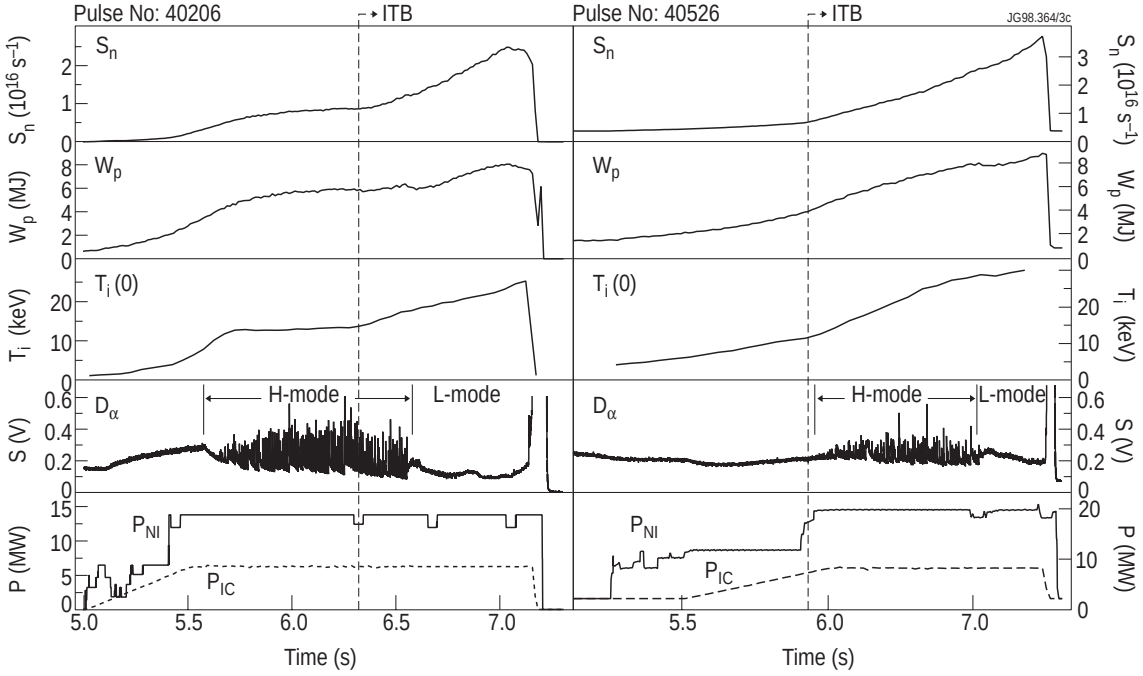

Fig.6: Discharges with ITB in ELMy H-mode. Fusion neutron rate S_n, diamagnetic energy W_p, central ion temperature $T_i(0)$, D_α emission and heating powers from NBI and ICRH. a) ITB formation after the H-transition (left side, pulse No. 40206). b) H-mode transition shortly after ITB formation (right side, pulse No. 40526).

early after reaching full power input from NBI and ICRH. After a long delay, with the ELM amplitude slowly growing at constant total power input, a bifurcation to increasing fusion rate (S_n) and total energy content (W_p) starts with the ITB formation at 6.3 s. A back-transition to L-mode is triggered at 6.5 s. Fusion neutron rate, plasma energy content and central ion temperature continue to rise during the L-mode phase until the final disruption occurs. In pulse No. 40526 (Fig. 6b) a delayed step-up in high power heating was instrumental to induce an ITB first, shortly followed by a transition to ELMy H-mode. The subsequent evolution with L-mode back-transition and continuous rise in S_n and W_p is similar to the previous discharge. The typical temperature profile evolution in this type of discharges is seen from Fig. 7. Core ion and electron temperatures start increasing after the ITB forms in the ELMy H-mode phase. The peripheral temperatures remain constant at their H-mode pedestal. After the L-mode back-transition, the edge temperatures decrease while the peaking in the core and the expansion of the ITB continue until an MHD mode is destabilised. The H-mode in these discharges can not be maintained due to reduced power flow from the core to the edge after the ITB formation. Off-axis heat deposition outside the ITB location might be a possible way to keep the plasma in ELMy H-mode.

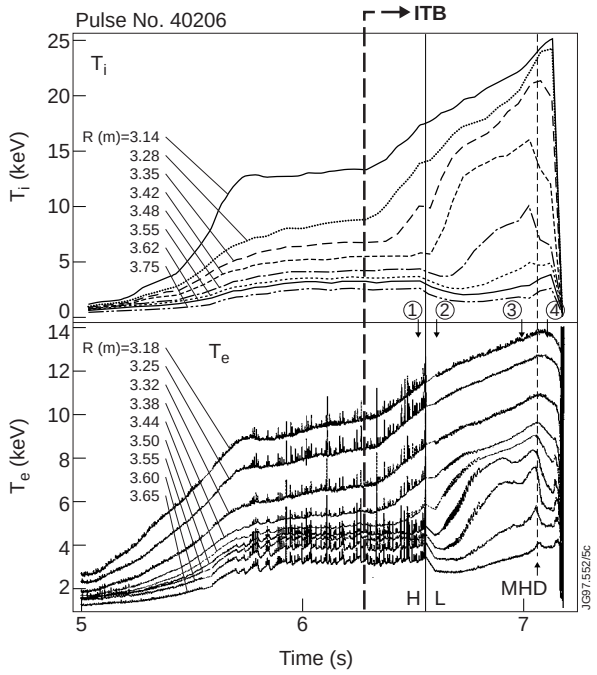

Fig.7: Time evolution of ion and electron temperatures across the plasma cross section in the ITB ELMy H-mode of Fig. 6a.

4.2 Steady-state ELMy H-modes with Internal Transport Barriers

Stable operation at high performance with the combination of ITB and H-mode depends critically on ELM amplitude and frequency. Two discharges with two different approaches to a steady-state ITB/ELMy H-mode are documented in Fig.'s 8 and 9.

Pulse No. 38437 (Fig. 8) evolves along the Optimised Shear high performance route with an early ITB formation in L-mode and a subsequent transition to ELM-free H-mode. The D_α emission is plotted in two different scales in Fig. 8 to bring out more clearly the different phases. The broad spread in the L-mode reflects the low frequency MHD mode seen from the 1 kHz pick-up signal. A short high frequency burst (seen on the 60 kHz signal) precedes the H-mode transition at 6.93 s. After a short ELM-free H-mode distinct ELMs of moderate amplitude appear and rapidly assume a more regular pattern. Fusion rate and energy content reach a flat top in this phase. Ion and electron temperatures saturate in the core and at the edge. Both, the increase in the pressure pedestal at the edge and the peaking in the core are thereby restrained. The MHD activity reverts to a low level, both in the low and high frequency range. This steady-state phase is only finished when the heating power from NBI is switched off.

Pulse No. 40542 (Fig. 9) forms an ITB early already at the end of the first high power heating step at 5.4 s. The discharge transits slowly from L-mode into an ELMy H-mode after a slight reduction of both NBI and ICRH power. The ELM amplitude as seen from the D_α emission is quenched at 6.5 s as a result of nickel tracer injection by laser blow-off for particle transport studies. The related enhanced radiation cooling reduces the conducted power flow through the plasma boundary and hence the edge pressure pedestal. Regular small amplitude

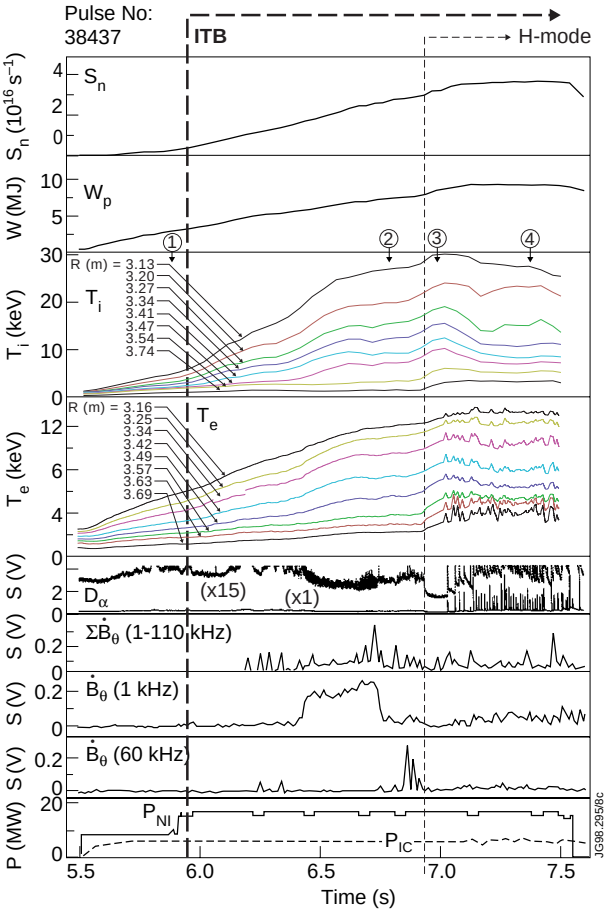

Fig.8: Steady-state discharge with ITB in ELMy H-mode. Fusion neutron rate S_n, diamagnetic energy W_p, ion and electron temperatures, D_α emission, magnetic pick-up signals and heating powers.

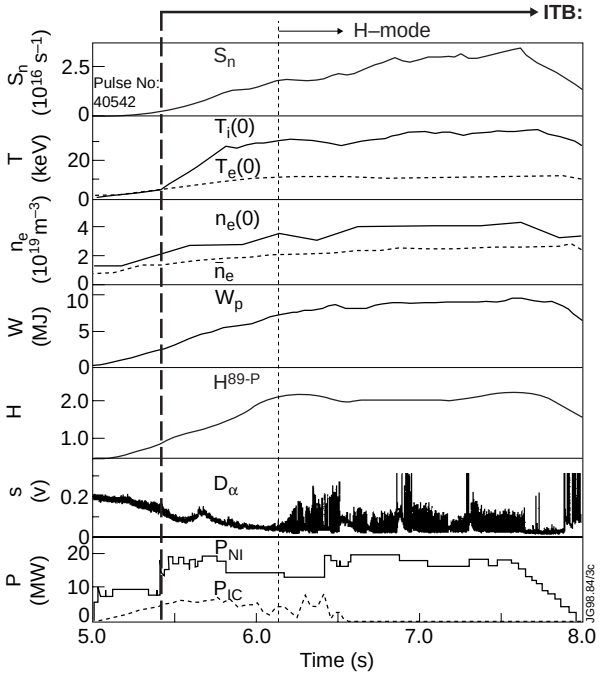

Fig.9: Steady-state discharge with ITB in ELMy H-mode. Fusion rate neutron S_n, central ion and electron temperatures, electron density, diamagnetic energy W_p, H-factor, D_α emission and heating powers.

ELMs persist then for the remaining duration of the high power heating phase. Occasional bursts are related to variations in the NBI power. Steady-state conditions with constant high ion and electron temperatures, densities and total energy content are reached. The line averaged density is still gradually rising due to the fuelling from NBI slightly exceeding the particle losses. The H-factor is maintained at $H^{ITER\ 89\text{-}P} \approx 2$ for a period of order four energy confinement times ($\tau_E \approx$ 0.45 s). The fusion neutron rate is still slightly increasing and reaches a value of $S_n = 3.3 \times 10^{16} s^{-1}$ at the end of the high power heating phase. Only the ramp-down of the NBI power at 7.5 s ends the quiescent high performance phase.

4.3 Profile Evolution

The characteristic evolution of the ion temperature profile in the combined ITB/ELMy H-mode operation is documented in Fig. 10 for discharge Pulse No. 38437 (Fig. 8). The ITB formation leads to strong peaking inside about half radius (time slice 2). The transition to ELM-free H-mode adds an edge pedestal and raises also the core temperatures (time slice 3). With the subsequent transition into ELMy H-mode (time slice 4), the overall peaking is reduced by broadening the core gradient region in the ITB and connecting smoothly to the edge pedestal.

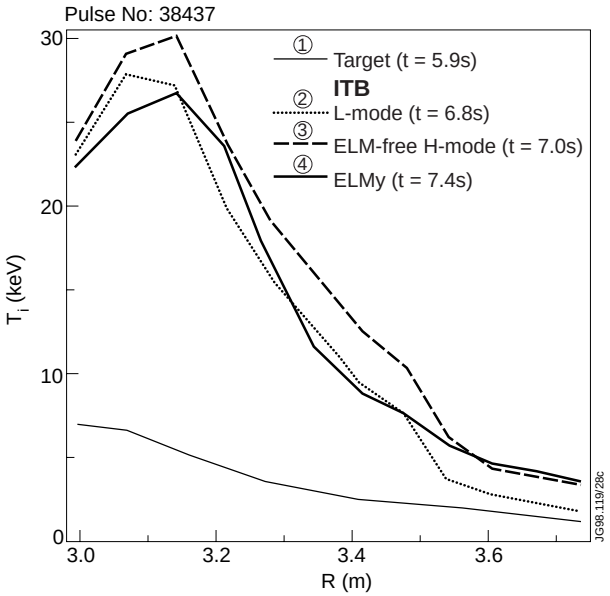

Fig.10: Ion temperature profiles in the various confinement phases of the ITB/H-mode discharge of Fig. 8.

The evolution of temperature, density and q-profiles for the long flat-top discharge pulse No. 40542 (Fig. 9) is summarised in Fig. 11. Ion and electron temperature profiles remain both strongly peaked inside the ITB also during the ELMy H-mode phase. The foot of the ITB has expanded out to about 2/3 of the plasma radius. The electron density profile shows less peaking. The q-profile is still slowly evolving, with the central values in a broad low shear region decreasing towards 1. Profile control with non-inductive current drive in the high power phase would be required to fully stop this evolution. The time evolution of the ITB location as defined by the outer footpoint of the steep gradient region (maximum of the second derivative) for electron and ion temperatures is shown in Fig. 12 together with contour lines for the q-profile as determined from the equilibrium reconstruction with the EFIT code [14]. Both ions and electrons form an ITB at the same radius. After a strong expansion from r/a ≈ 0.25 to r/a ≈ 0.65, the outer footpoint of the ITB ties up with the q=2 surface. From 6.0 s to the end of the high power heating at 7.5 s, ITB radius and the q-profile show only small differential changes.

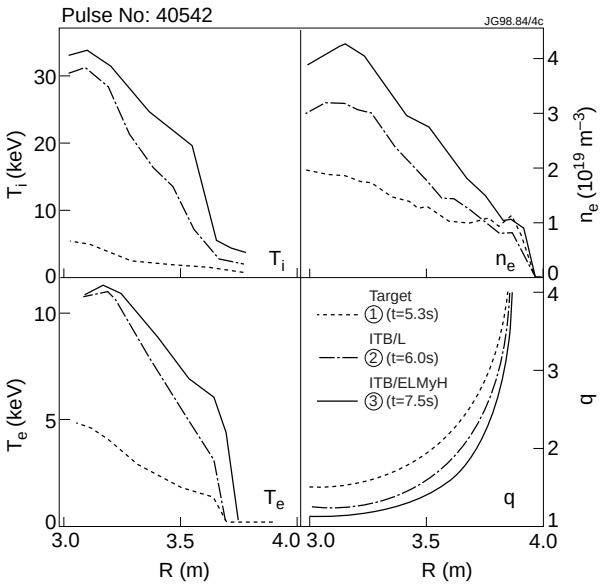

Fig.11: Ion and electron temperature, density and q-profiles in the various confinement phases of the ITB/H-mode discharge of Fig. 9.

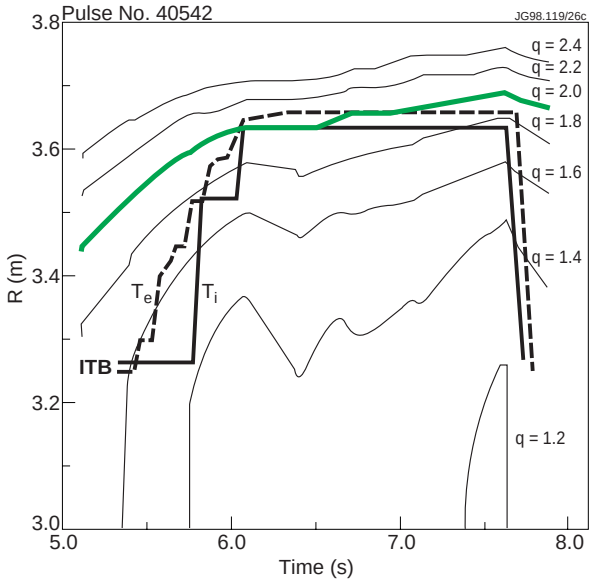

Fig.12: Time evolution of ion and electron temperature ITBs together with contour lines of the q-profile in the discharge of Fig. 9.

The relaxation of the pressure profile evolution results also in a freezing of the bootstrap current profile as shown in Fig. 13 from TRANSP transport code calculations. The bootstrap current remains peaked in the core region due to the peaked pressure profile. Maintaining a wide central region of low magnetic shear with q>1 would require additional non-inductive current drive off-axis to compensate for the too centrally peaked bootstrap current. The total non-inductively driven current from NBI and the bootstrap effect amounts to about 30 % of the total plasma current during the stationary phase of the discharge shown in Fig. 9. The bootstrap fraction remains low due to the low beta of $ß_N < 1.5$ in this discharge. For full steady-state operation this fraction needs to be increased by at least a factor 2. This should be achieved with an increase in the beta limit by widening of the flat shear region with current profile control from LHCD. In these conditions the full available heating power from NBI and ICRH can be applied in a later high performance stage with a wide ITB. Transport code modelling calculations predict for JET experimental scenarios an improvement by about a factor 2 in the beta limit with current profile control.

The approach of temperature, density and current profiles to stationary conditions is documented in Fig. 14. There the normalised time derivatives for central and volume averaged values, (dT(0)/dt)/T(0), (dn(0)/dt)/n(0) and (d<T>/dt)/<T>, (d<n>/dt)/<n>, are plotted versus time. The current profile is characterised by the time derivatives of central q-value and the internal inductance l_i, (dq(0)/dt)/q(0) and $(dl_i/dt)/l_i$. The strongest profile changes occur

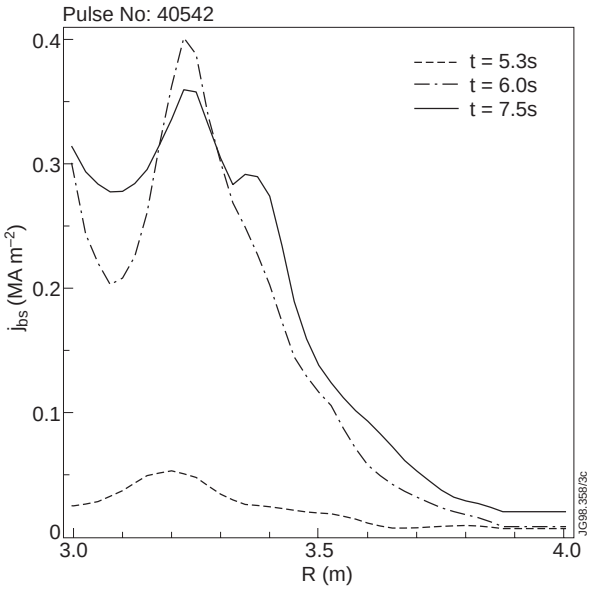

Fig.13: Bootstrap current profiles as determined with the TRANSP transport code for the times of the profiles shown in Fig. 12.

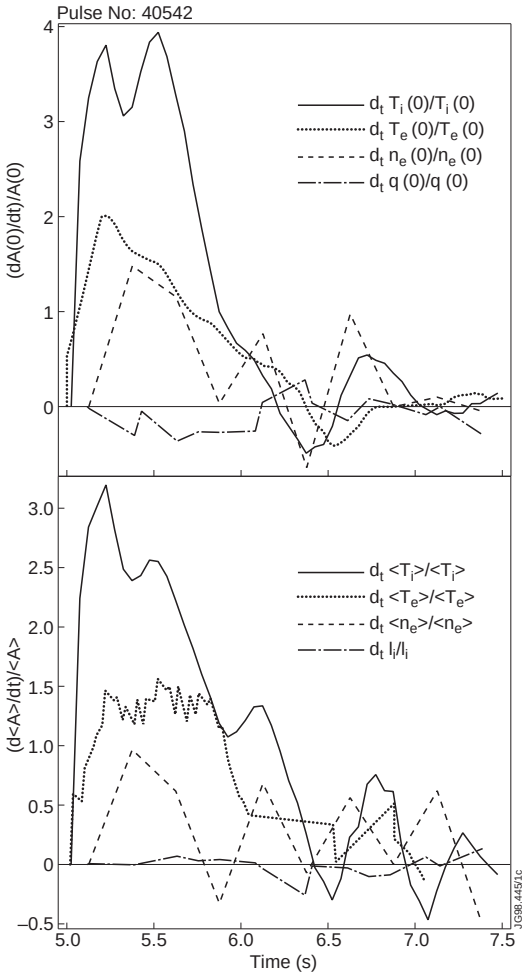

Fig.14: Time evolution of normalised time derivatives for central and volume averaged temperatures and density as well as central q-value and internal inductance l_i in the discharge of Fig. 9.

after the ITB formation in the initial L-mode phase. The change is largest in the ion temperature profile. The current profile shows only small changes. All profiles relax after the edge transition into ELMy H-mode and the time derivatives diminish then strongly. This relaxed state is reached at ~ 6.5 s, about 1 s after the start of the full power at 5.4 s. The relaxation time corresponds to about two energy confinement times ($\tau_E \approx 0.45$ s at t = 6.5 s), about one particle confinement time ($\tau_p \approx 0.8$ s at t = 6.5 s) and about 10% of the characteristic time scale for current profile changes. At the end of the high power heating phase the discharge comes close to stationary conditions.

4.4 Energy Transport

The local heat transport has been analysed with the TRANSP code. Measured energy content and neutron rate are well reproduced by the code calculations as seen in Fig. 15. The thermonuclear neutron production $S_{n,th}$ dominates in the late high performance phase with about 2/3 of the total neutron rate. Beam-target reactions ($S_{n,bt}$) follow while the beam-beam contribution ($S_{n,bb}$) is small.

The ion heat conductivity drops first in the central region after the ITB formation. The improved confinement region then expands radially out to about 2/3 of the plasma cross section (Fig. 16). In the core region the ion heat conductivity falls to the neo-classical level with values of $\chi_{i,exp} \leq 0.1$ m^{2}s^{-1}. The neo-classical heat diffusivity in Fig. 16 has been calculated with the Chang-Hinton formula, not including orbit squeezing effects. The H-mode further reduces the heat conductivity in the peripheral region by about a factor 3 to $\chi_{i,exp} \approx 3$ m^{2}s^{-1}.

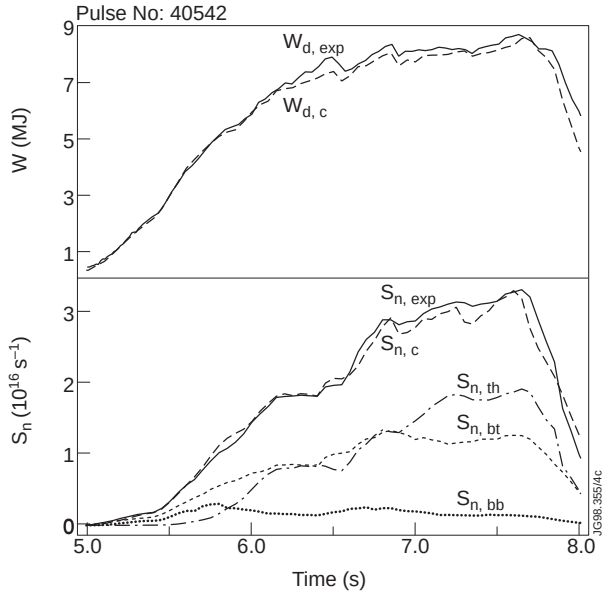

Fig.15: Comparison of experimental diamagnetic energy content, $W_{d,exp}$ and neutron rate, $S_{n,exp}$ with the quantities from TRANSP transport code calculations.

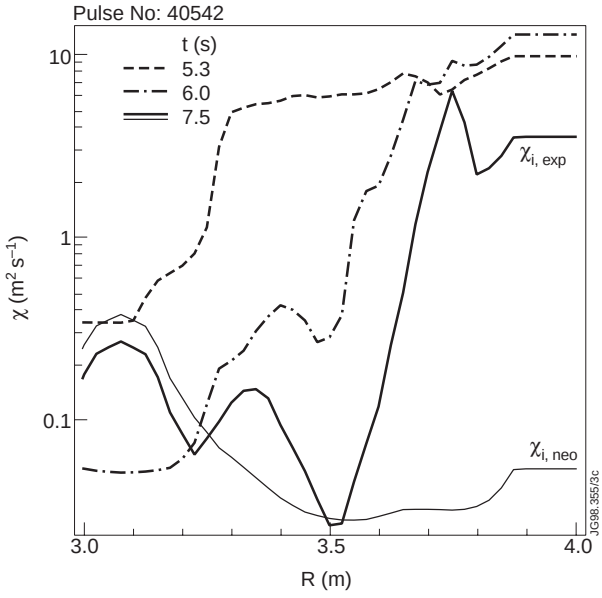

Fig.16: Ion heat conductivity from TRANSP transport code calculations for the experiment ($\chi_{i,exp}$) and neoclassical values ($\chi_{i,neo}$).

Electron heat conductivities are reduced as well over the whole plasma cross section and show an ITB at the same location as seen from the ion heat conductivity profile. The reduction in the electron heat conductivity, however, is much smaller than in the ion heat conductivity. Inside the ITB, the electron heat diffusivity χ_e drops typically by a factor 5, while $\chi_{i,}$ falls by up to two orders of magnitude. This different behaviour in ion and electron heat conductivities is observed both during the ITB/L-mode and in the ITB/H-mode phase. It might indicate different stabilisation of the turbulence sources responsible for anomalous electron and ion heat transport. Dissipative trapped electron (DTE) modes are a possible mechanism for the persisting anomalous electron heat transport.

In the ITB/ELMy H-mode no degradation of the ITB with the related local rise of the heat conductivities inside the core gradient region is seen, as it is usually observed after transitions from ITB/L-mode to ITB/ELM-free H-mode [14]. The ITB/ELMy H-mode provides a sustainable superposition of internal and external transport barriers in the radial energy transport. The core transport is reduced below the values obtained in conventional ELMy or ELM-free H-modes and reaches the neo-classical level for the ions.

4.5 Particle Transport

Accumulation of impurities in the core is a major threat to improved core confinement regimes. The local transport of heavy and light impurities therefore has been studied in detail in the different regimes of operation with Optimised Shear [15]. Tracer impurities of different species have been injected with the laser blow-off (LBO) technique. The temporal evolution of line emission from two high ionisation stages of nickel is compared in Fig. 17 for injection into an ITB/ELMy H-mode and into an ITB/L-mode. In the ITB/ELMy H-mode (pulse No. 40542, Fig. 17/left side) the line emission decays exponentially after the initial increase following injection. In the ITB/L-mode (pulse No. 40572, Fig. 17/right side) only the lower ionisation state of Ni^{25+} decays. The higher ionisation stage of Ni^{26+} continues to rise throughout the whole high core confinement phase. Tomographic reconstruction of the 2D distribution of soft X-ray emission, mainly determined by the Ni emission, shows a hollow annular distribution of the maximum emissivity in the region of the steep gradient region for the ITB/L-mode. In the ITB/ELMy H-mode case the emissivity profile is centrally peaked throughout. The core radiation rises continuously after Ni injection in the ITB/L-mode. In the ITB/ELMy H-mode pulse, on the other hand, the core radiation increases only transiently and falls then back to the initial level. No high-Z impurity accumulation is seen in this case.

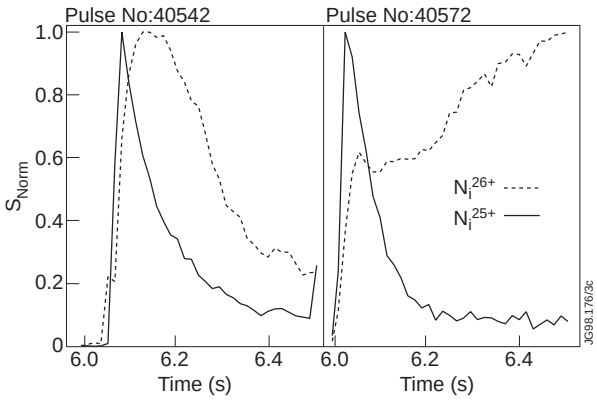

Fig.17: Temporal evolution of the line emission from two highly ionised nickel ions after injection into an ITB/ELMy H-mode (left side) and an ITB/L-mode (right side).

The behaviour of light impurities is determined from charge exchange measurements of the carbon density profile. The time evolution of the radial distribution of the carbon concentration for both discharges is shown in Fig. 18. In the ITB/L-mode the carbon density profile is gradually peaking, with the carbon concentration in the centre increasing over the whole period of improved core confinement (Fig. 18, lower part). In the ITB/ELMy H-mode (Fig. 18, upper part) the carbon profile remains flat and the carbon concentration in the centre decreases with increasing electron density.

Particle transport shows therefore a marked difference between ITB/L-mode and ITB/ELMy H-mode. The strong ITB in a discharge where the outer part resides in L-mode limits inward penetration of heavy impurities across the ITB but gives rise to accumulation of the residual impurities inside the ITB. The ELMs in the outer part of an ITB/ELMy H-mode, on the other hand, keep the radial particle transport at a higher level and prevent core accumulation of low- and high-Z impurities. Diffusion coefficients and inward pinch velocity derived from the Ni profiles for both types of discharges are shown in Fig. 19. In the ITB/L-mode, diffusion inside the ITB is strongly reduced and the transport is mainly convective with an inward pinch. In the ITB/ELMy H-mode the transport is diffusion dominated, with a diffusion coefficient of D $\approx$ 0.5 m^2s^{-1} inside the ITB and rising to D $\approx$ 4 m^2s^{-1} outside the ITB.

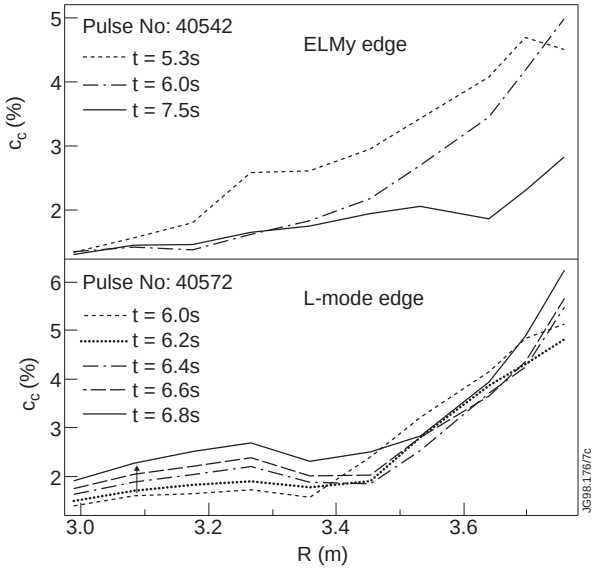

Fig.18: Radial profiles of the carbon concentration in an ITB/ELMy H-mode (top) and an ITB/L-mode (bottom) discharge.

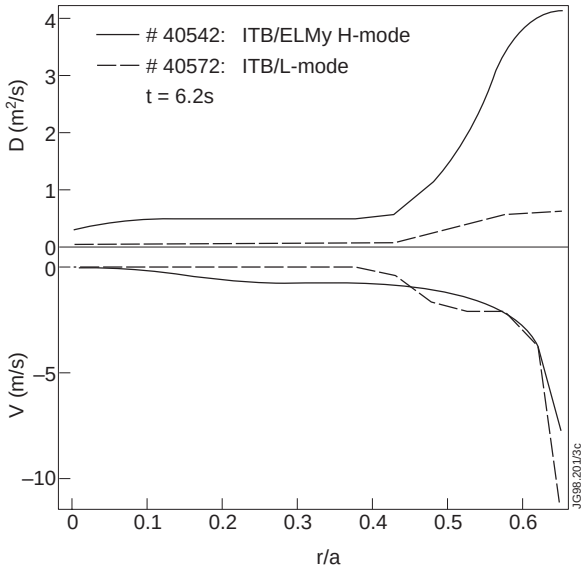

Fig.19: Radial profiles of diffusion coefficient and inward velocity as derived from LBO Ni injection for two types of Optimised Shear discharges with ITB.

The improvement of particle confinement is therefore less pronounced than the reduction in ion heat conductivity. Electron heat conductivities, on the other hand, are also much less reduced than the ion heat conductivity in this case. The behaviour of the particle transport is consistent with a dependence of the diffusion coefficient on a combination of ion and electron heat conductivity, as used in the transport model developed for JET Optimised Shear discharges [16]:

$$D \sim \chi_i \chi_e/(\chi_i + \chi_e)$$

The difference in ion and electron heat transport reduction therefore allows a partial decoupling of energy and particle confinement. Strongly peaked temperature profiles can thus be combined with modestely peaked density profiles. The moderate improvement in particle confinement prevents impurity accumulation in conditions of improved core confinement.

4.6 MHD Stability

MHD instabilities have limited the peak performance of Optimised Shear discharges. A pressure driven n=1 ideal kink mode may grow unstable in high performance phases with an ITB and an L-mode edge and lead to disruptions [11]. The disruptive termination could be avoided by broadening the gradient zone and adding an edge pedestal with an H-mode transition as discussed in Section 2.2.

The ELMy H-mode raises the marginal stability limits as it reduces the global pressure peaking and constrains the edge pressure pedestal afflicting the ELM-free H-mode. The time evolution of the normalised beta value $ß_N$ in the experiment and the stability boundaries from MHD stability code calculations is shown in Fig. 20 for the Optimised Shear DB mode discharge of Fig. 9. After the L-H transition around 6.1 s the rate of rise of beta decreases. The beta limit, on the other hand, increases gradually due to an increase of the pressure outside the ITB and the resulting decrease of the pressure peaking. The stable operation range thereby widens and the beta value rising in the experiment stays away from the marginal stability boundary. The pressure peaking factor ß(0)/<ß> decreases gradually as shown in Fig. 21. Toroidal and poloidal beta values, $ß_t$ and $ß_p$, rise and approach a flat top in the later phase of the DB mode until reduction of the NBI power input.

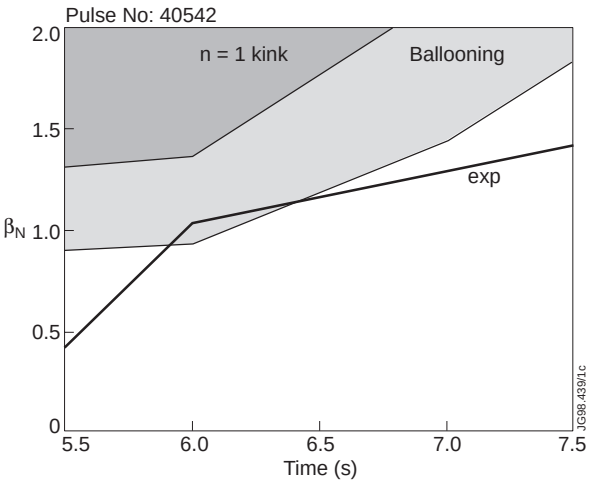

Fig.20: Temporal evolution of normalised beta $ß_N$ in the experiment and stability boundary from MHD stability code calculations for an ITB/ELMy H-mode discharge in DT.

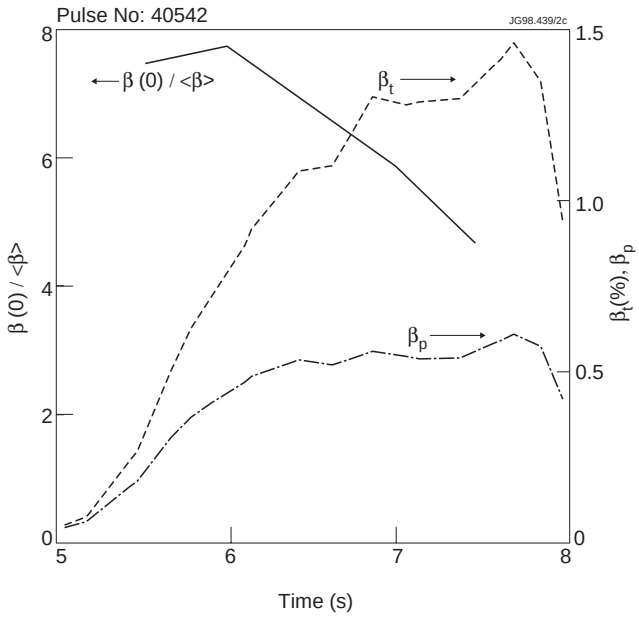

Fig.21: Pressure peaking factor ß(0)/<ß>, toroidal beta $ß_t$ and poloidal beta $ß_p$ in an ITB/ELMy H-mode discharge in DT.

The MHD stability calculations for this discharge identify the ballooning instability as the lowest limit to beta, as the shear is slightly positive in the core region of the peaked pressure profiles. With a minor modification to the current profile, as shown in the experiment [7], negative central magnetic shear can be obtained. The ballooning modes are then completely stabilised. The beta limit is then determined by the marginal stability boundary of the pressure driven global n=1 kink mode shown in Fig. 20. This mode has been indeed the dominating limitation to performance in the Optimised Shear scenario. In the DB mode analysed here the beta limit due to kink modes rises above 2 about 0.5 s after the H-mode transition. At the end of the high power heating phase the beta limit has increased above 3. In these conditions the performance is power limited and no longer stability limited. The input power therefore can be increased again in this phase with a large stability margin.

Pressure profile control by real time control of the power deposition profile on JET has allowed to attain transiently normalised beta values up to $ß_N = 1.8$. Transport code modelling studies have shown that simultaneous pressure and current profile control may raise the beta limit up to $ß_N = 3.2$ in DB mode discharges on JET [17].

4.7 Comparison of Double Barrier Mode with Conventional ELMy H-mode

Double Barrier modes with an ITB and an ELMy H-mode edge have been readily obtained on JET in deuterium-tritium discharges during the DTE-1 campaign. The lower H-mode threshold power in tritium has privileged earlier H-mode transitions. Heavy restrictions on the thermonuclear neutron production necessitated, however, a priority choice in favour of short duration high performance pulses as obtained in the ITB/L-mode with a subsequent ELM-free H-mode [18]. Discharges transiting into ELMy H-mode with the resulting lower rate of rise of the fusion power have therefore been stopped by real time control of the heating power, monitoring the difference between requested and achieved fusion performance. The ITB/ELMy H-mode comes close to steady-state conditions in many important quantities, however, already during the experimentally explored phase. A comparison with the conventional sawtoothing ELMy H-mode shows the potential of the DB mode for long pulse operation.

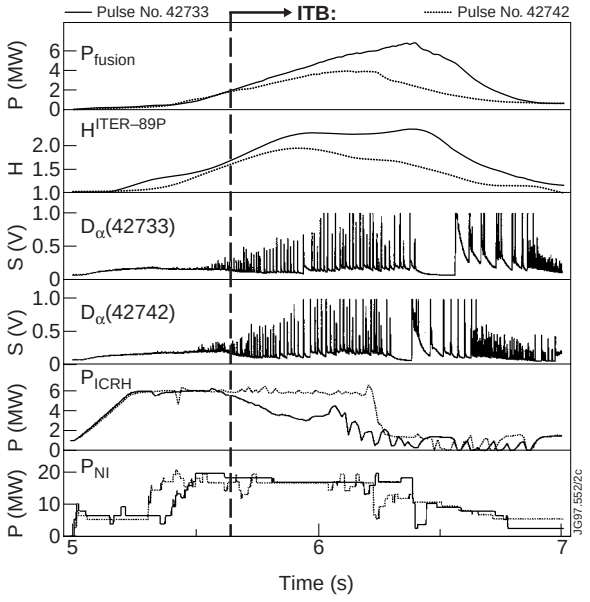

Fig.22: Comparison of two ELMy H-modes in deuterium-tritium, pulse No. 42733 with ITB, pulse No. 42742 without ITB.

A DB mode DT discharge in ITB/ELMy H-mode is compared in Fig. 22 with an ELMy H-mode without ITB in the same plasma configuration with similar power input. The ELMy H-mode phase starts in both discharges at about

the same time, with the ELMs gradually growing in amplitude and saturating after ~ 0.5 s. In a confinement bifurcation, pulse No. 42733, with slightly higher initial NBI power, forms an ITB at 5.65 s, briefly after the H-mode transition. Fusion power and H-factor subsequently increase to about 50% higher values than in the pulse No 42742 without ITB by the time the power is turned down, at 6.2 s. The bifurcation in ion and electron temperature evolution is seen from Fig. 23. In the ITB/ELMy H-mode central ion temperatures rise up to 25 keV compared with 15 keV in the pulse without ITB. The edge temperatures remain similar in both cases. Radial profiles of ion and electron temperature and density at the begin of high power heating (5.3 s), before the bifurcation (5.6 s) and before ramp-down of heating (6.2 s) are compared in Fig. 24. Ion and electron temperature profiles peak strongly inside the ITB in the case of the ITB/ELMy H-mode. The density profiles develop similarly in both ELMy H-mode discharges, with and without ITB. This decoupling between strong temperature peaking and moderate density peaking has been observed consistently in ITB/ELMy H-modes in deuterium and DT mixtures.

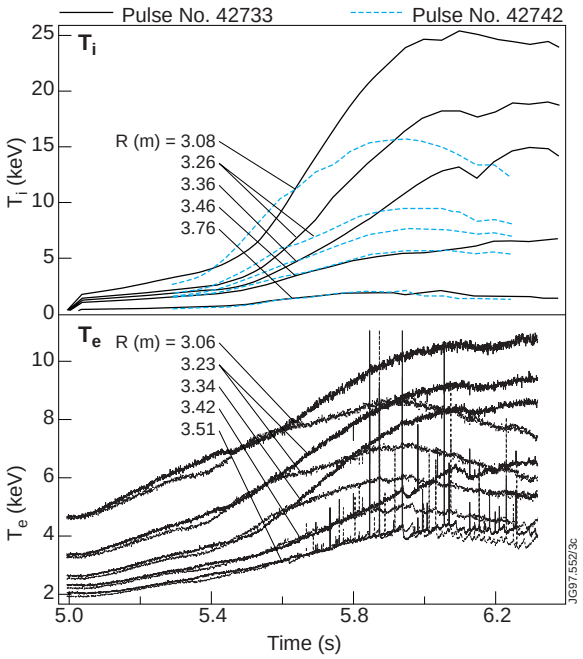

Fig.23: Temporal evolution of the ion temperature across the plasma cross section in the ITB/ELMy H-mode and in the conventional ELMy H-mode of Fig. 22.

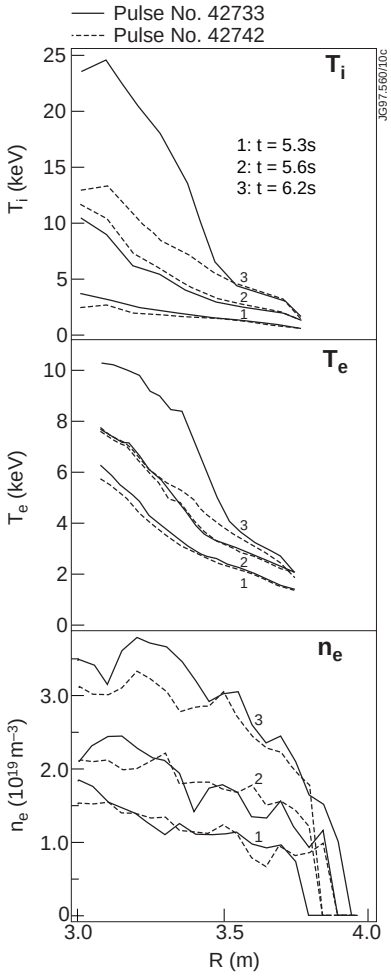

Fig.24: Radial profiles of ion and electron temperature and density at the begin of high power heating (5.3 s), before the bifurcation (5.6 s) and before ramp-down of heating (6.2 s) for the ITB/ELMy H-mode and in the conventional ELMy H-mode of Fig. 22.

Transport analysis with the TRANSP code for both discharges shows the bifurcation in the core ion heat conductivities as presented in Fig. 25. In the ITB/ELMy H-mode the ion heat conductivity falls in the central region to values $\chi_{i,exp} \approx 0.2\ m^2 s^{-1}$ and reaches the neo-classical level.

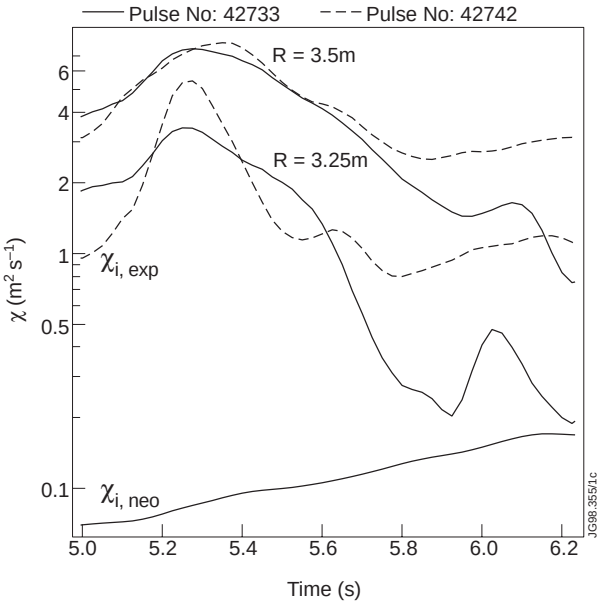

Fig.25: Time evolution of experimental and neo-classical ion heat conductivity in the ITB/ELMy H-mode and in the conventional ELMy H-mode of Fig. 22.

The difference between the two pulses seems to be related to the different evolution of the q-profiles. In the discharge which remains in the conventional ELM´y H-mode without forming an ITB, the q-values remain above 2 throughout the high performance phase. The location of the q=2 surface has been found to be a critical parameter for the maximum performance which can be achieved in the Optimised shear Scenario [10]. In discharge #42733, the q=2 surface appears already during the pre-heating phase and has expanded to r/a ≈ 0.5 at the beginning of the high power heating phase.

The q-profile has been linked to the confinement in a transport model developed at JET for Optimised Shear discharges with ITBs and external H-mode transport barriers [16]. The model assumes suppression of long wavelength turbulence by a combined action of magnetic shear and shear in poloidal rotation, the latter largely produced by steep radial pressure gradients. Low magnetic shear provides a break-up of toroidal coupling, thereby reducing the growth rate. Poloidal rotational shear is expected to lead to the final stabilisation when the *ExB* shearing rate exceeds the maximum linear growth rate of ion temperature gradient (ITG) modes [19]. The model has been used in the 1.5D predictive/interpretative transport code JETTO to simulate the two ELMy H-modes, with and without ITB formation, as presented in Fig.'s 22-24. The ion heat conductivity profiles in both discharges are well reproduced by the modelling calculations as shown in Fig. 26. The transport model

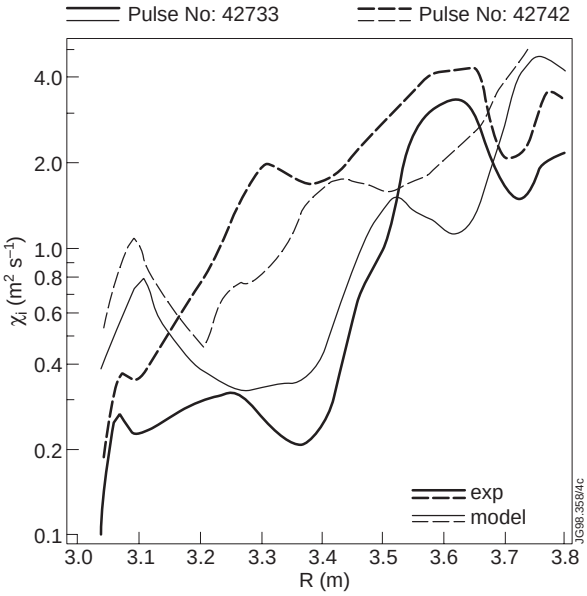

Fig.26: Radial profiles of ion heat conductivities from experiment and transport code modelling for the ITB/ELMy H-mode and the conventional ELMy H-mode of Fig. 22 at t = 6.2 s (time slice 3 in Fig. 24).

therefore describes correctly the core confinement bifurcation and subsequent sustainment of an internal transport barrier in an ELMy H-mode.

The Optimised Shear discharge of Fig. 22 in Double Barrier mode is compared in Fig. 27 with the steady-state ELMy H-mode which produced the highest fusion energy on JET [20]. Similar total power input from NBI and ICRH is applied in both cases. The main parameters of the two discharges are given in Table 1. The same normalised beta value of $ß_N = 1.5$ is obtained in both cases. About 50% higher fusion power is reached in the DB mode, with $P_{fus} = 6.8$ MW at t = 6.35 s before the NBI power is ramped down, compared with $P_{fus} = 4.5$ MW in pulse No. 42982. Also the H-factor rises to appreciably higher values, with $H^{ITER-89} \approx 2.3$ in the DB mode, compared with $H^{ITER-89} \approx 1.7$ in the conventional ELMy H-mode. The fusion triple product is more than a factor two higher in the DB mode with $n_i(0)T_i(0)\tau_E = 4.4$, compared with $n_i(0)T_i(0)\tau_E = 1.9$ in the conventional ELMy H-mode. The fusion gain reaches double the value with Q = 0.4, compared with Q = 0.2 in the conventional ELMy H-mode. Three values for the fusion gain Q are plotted in Fig. 27, using either only the ratio of input power to fusion power produced or correcting for the rate of change in the energy content (dW_p/dt) and contributions from α-particle heating (P_α), respectively. At the approach to steady-state conditions, the fusion power in the DB mode discharge had to be ramped down due to stringent limitations on the neutron production. Long pulse demonstration has been limited in the DTE-1 campaign on JET to the conventional ELMy H-mode.

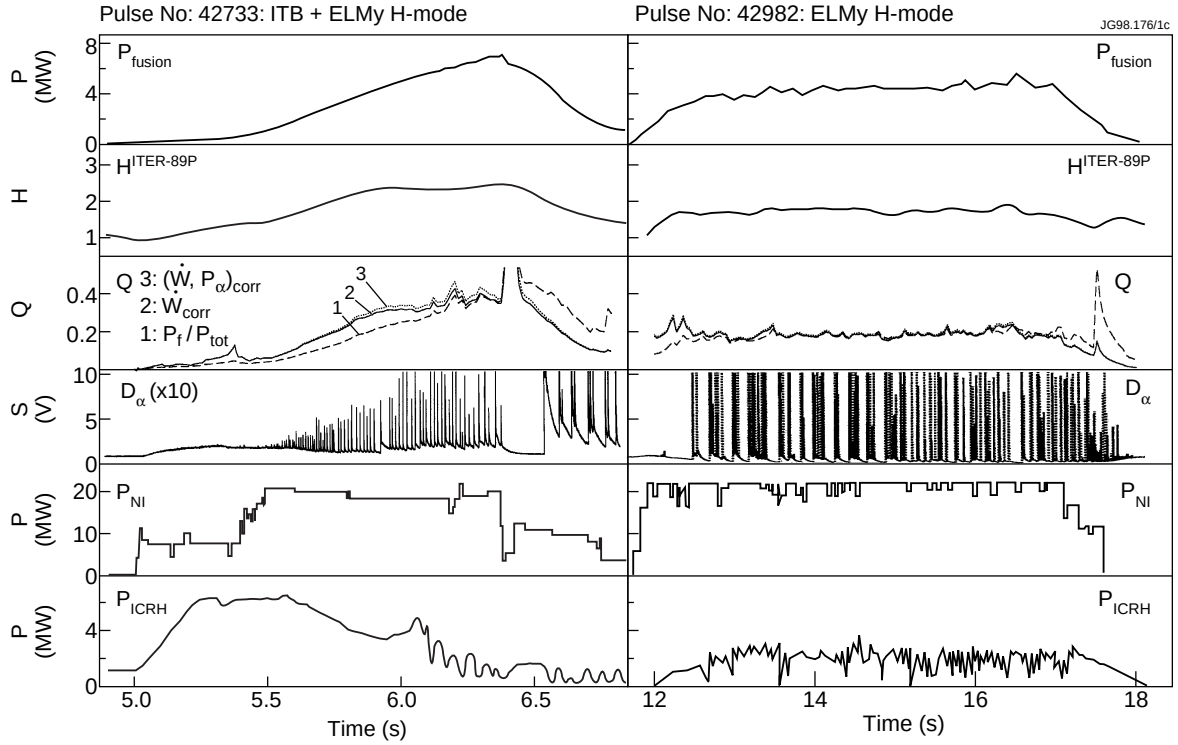

Fig.27: Comparison of two DT pulses on JET, in the Optimised Shear regime with Double Barriers (pulse No. 42733) and in conventional ELMy H-mode (pulse No. 42982).

Table 1: Parameters in JET DT discharges in conventional ELMy H-mode (pulse No. 42982) and in Double Barrier mode with Optimised Shear (pulse No. 42733).

	Pulse No. 42982 (ELMy H-mode)	**Pulse No. 42733 (Double Barrier)**
I_p (MA)	3.8	3.0
B_t (T)	3.9	3.45
q_{95}	3.5	4.0
δ	0.2	0.25
κ	1.7	1.8
P_{NI} (MW)	21.1	16.6
P_{ICRH} (MW)	1.8	1.8
P_{tot}(MW)	22.5	16.4
n_e ($10^{19}m^{-3}$)	6.8	3.3
n_i (0) ($10^{19}m^{-3}$)	5.6	3.3
T_e (0) (keV)	8.3	14.0
T_i(0) (keV)	8.5	24.0
W_{dia} (MJ)	10.3	8.8
β_N	1.5	1.5
τ_E (s)	0.4	0.55
H-89	1.7	2.3
H-93	0.6	1.1
$n_i(0)T_i(0)\ \tau_E$($1020m^{-3}$ keVs)	**1.9**	**4.4**
P_{fusion} (MW)	**4.5**	**6.8**
Q	**0.2**	**0.4**

The ELMs are of much smaller amplitude in the steady-state DB mode than in the steady-state conventional ELMy H-mode, as seen from the D_α emission traces in Fig. 27. The energy loss in a single ELM is typically an order of magnitude smaller in the DB mode. This is of particular importance in view of the critically high peak power load on the divertor plates with the actually considered standard ignition scenario in ELMy H-mode on ITER.

5. SUMMARY AND CONCLUSIONS

Optimised Shear plasmas have achieved the record fusion performance in deuterium plasmas on JET with the formation of an Internal Transport Barrier and the superposition of an external transport barrier in H-mode. Different modes of operation with single or combined transport barriers have been explored. The peak performance with ITB is limited by MHD modes. In high performance discharges with an L-mode edge a kink mode driven by excessive pressure peaking leads to disruptions. With the superposition of an H-mode edge disruptions are avoided but a soft roll-over is still encountered.

The high performance phase with ITB has been extended either with a slight degradation of the ITB by local MHD activity or by the combination with an ELMy H-mode which limits both, excessive core peaking and the build-up of an edge pressure pedestal. This Double Barrier mode with an internal transport barrier and an ELMy H-mode edge has allowed to maintain peaked pressure profiles and high H-factors and fusion rates for several energy confinement times. Steady-state conditions have been closely approached in temperature and density profiles, and the current profile is only slowly evolving. The ion heat conductivity is strongly reduced across the whole plasma cross section in the Double Barrier mode, in the core down to the neo-classical level. Particle transport is less reduced than ion heat transport. Therefore strongly peaked temperature profiles combine with moderately peaked density profiles in the Double Barrier mode. The level of remaining particle outward diffusion prevents impurity accumulation. This should alleviate the problem of ash removal from a high confinement core in a burning plasma. The peak power load deposited on the divertor plates is strongly reduced with the smaller ELMs in the Double Barrier mode.

The confinement improvement in the Double Barrier mode can be consistently explained with a transport model developed on JET for Optimised Shear discharges. The reduction of the radial transport there is linked to turbulence stabilisation by the combined action of low magnetic shear and shear in poloidal rotation mainly produced by a steep pressure gradient.

High fusion power of 6.8 MW has been achieved with the Double Barrier mode in experiments with deuterium-tritium on JET. The performance is superior to the conventional sawtoothing steady-state ELMy H-mode. About a factor two higher fusion triple product and fusion gain Q have been attained in the Double Barrier mode.

Long pulse steady-state operation in the Double Barrier mode still needs to be demonstrated. This requires active current profile control during the high performance phase with off-

axis non-inductive current drive to maintain a wide central region of low magnetic shear against the contracting effect of the bootstrap current peaked in the core region of steep pressure gradients. The existing Lower Hybrid current drive system will be used for this purpose in future experiments on JET.

Future experiments on JET aim at the improvement of tokamak operation with Optimised Shear scenarios in the Double Barrier mode in three stages. First, an extended pulse duration at high performance with high core pressure will allow high quality α-particle heating physics studies in another campaign with deuterium-tritium discharges. Second, physics studies of the Double Barrier mode and the establishment of scaling relations should provide the basis for a viable alternative operation scenario in an improved ELMy H-mode on ITER. Third, optimisation of the bootstrap current generation at high performance should explore the potential for steady-state operation of a tokamak reactor with minimum need for external current drive.

Operational margins of ITER can be improved considerably with an increase of confinement quality and MHD stability as projected in modelling calculations for the Double Barrier mode based on JET experimental results [17]. Raising the H-factor to $H^{ITER-93} = 1.2$ and the beta limit to $ß_N = 2.6$ would allow to achieve ignition in ITER at or slightly below the Greenwald density limit [21]. This would relax on one of the most severe operation constraints of ITER. The time scales achievable on JET are consistent with Next Step requirements. A flat-top time of 6 s at high performance with Double Barriers in JET corresponds to 300 s, the envisaged burn time, in a presently discussed reduced version of ITER.

The combination of high core energy confinement, moderate particle confinement, sustainable plasma edge conditions and reduced divertor peak power load make the Double Barrier mode a promising candidate for operation in reactor conditions.

ACKNOWLEDGEMENTS

These results have been made possible only by the work of the whole JET team. Contributions of collaborators from TFTR, Princeton, USA and UKAEA, Culham, U.K. have been particularly valuable for this work.

REFERENCES

[1] Hugon, M. et al, Nucl. Fusion 32 (1992), 33.

[2] Levinton, F. M. et al., Phys. Rev. Lett. 75 (1995), 4417.

[3] Strait, E. J. et al., Phys. Rev. Lett. 75 (1995), 4421.

[4] Fujita, T., et al., Plasma Phys. and Contr. Nucl. Fusion Research 1997 (Proc. 16th Int. Conf., Montréal, 1996), Vol. I, IAEA, Vienna (1997), 227.

[5] Gormezano, C. and the JET Team, Plasma Phys. and Contr. Nucl. Fusion Research 1997 (Proc. 16th Int. Conf., Montréal, 1996), Vol. I, IAEA, Vienna (1997), 487.

[6] Lazarus, E.A., et al., Phys. Rev. Lett. 77 (1996), 2714.

[7] Söldner F.X., JET Team, Plasma Physics and Contr. Fusion 39, B353 (1997).
[8] Koide, Y. et al., Plasma Phys. and Contr. Nucl. Fusion Research 1994 (Proc. 15th Int. Conf. Sevilla, 1994), Vol. I, IAEA, Vienna (1995), 199.
[9] Sips, A.C.C. et al., Plasma Physics and Contr. Fusion 40, (1998), 1171.
[10] Gormezano, C. , et al., Phys. Rev. Lett. 80, 5544 (1998).
[11] Huysmans, G.T.A. et al., 24th Europ. Conf. on Contr. Fusion and Plasma Physics, Berchtesgaden 1997, Vol. I, 21.
[12] Huysmans, G.T.A. et al., to be published in Nucl. Fusion.
[13] Alper, B. et al., 24th Europ. Conf. on Contr. Fusion and Plasma Physics, Berchtesgaden 1997, Vol. I, 9.
[14] Baranov, Y., et al., to be published in Nucl. Fusion.
[15] Chen, H., et al., 25th Europ. Conf. on Contr. Fusion and Plasma Physics, Prague 1998, to be published.
[16] Parail, V., et al., to be published in Nucl. Fusion.
[17] Fischer, B., et al., Internal Report JET-R(98)05 (1998).
[18] Keilhacker, M., et al., to be published in Nucl. Fusion.
[19] Hahm, T.S., K.H. Burrell, Phys. Plasmas 2 (1995), 1648.
[20] Jacquinot, J., et al., to be published in Nucl. Fusion.
[21] Aymar, R., et al., Plasma Phys. and Contr. Nucl. Fusion Research 1997 (Proc. 16th Int. Conf., Montréal, 1996), Vol. I, IAEA, Vienna (1997), 3.